Solid State Electronics 145 (2018) 8–18

Contents lists available at ScienceDirect

Solid State Electronics

journal homepage: www.elsevier.com/locate/sse

Numerical modeling of reverse recovery characteristic in silicon pin diodes

Yusuke Yamashita*, Hiroshi Tadano

University of Tsukuba, Tsukuba, Ibaraki 305-8573, Japan

ARTICLE INFO

The review of this paper was arranged by Prof. A. Zaslavsky

ABSTRACT

A new numerical reverse recovery model of silicon pin diode is proposed by the approximation of the reverse recovery waveform as a simple shape. This is the first model to calculate the reverse recovery characteristics using numerical equations without adjusted by fitting equations and fitting parameters. In order to verify the validity and the accuracy of the numerical model, the calculation result from the model is verified through the device simulation result.

1. Introduction

Silicon pin power diodes are one of the most important components in power electronics. The main concern in such diodes is the large power loss, and attempts have been made to reduce this. Therefore, it is important to understand the behavior of the electrical characteristics of pin diodes. Especially, since the forward characteristic and the reverse recovery characteristic are strongly related to the power loss, several numerical models of pin diodes have been reported in previous studies.

For example, equations capable of calculating the carrier distribution in the i-layer have already been proposed [1,2], using which forward IV characteristics can also be calculated [3,4]. In addition, there exists a numerical reverse recovery model based on the change in the carrier density distribution in the i-layer [5,6]. Recently, since exhaustive analysis is possible, the numerical model of the reverse recovery was applied to SiC pin diodes [7,8]. However, since these models assume a resistive load, the reverse recovery current becomes constant within a certain period, and it is not possible to calculate the reverse recovery characteristic assuming an inductive load. For this reason, the carrier distribution model has been applied to circuit simulation to calculate reverse recovery characteristics [9]. Another study calculated the surge voltage from a numerical model [10], but other characteristic values such as the reverse recovery waveform, reverse recovery charge, and maximum reverse recovery current were not calculated. Therefore, there is no numerical model that calculates reverse recovery characteristics.

In our previous study, the reverse recovery characteristics were analyzed with a triangular current waveform by ignoring the tail current [11]. In this paper, we propose a new numerical model for computing the reverse recovery characteristics of the Si-pin diode with high accuracy including tail current, and report the result of verification using device simulation to demonstrate its accuracy of proposed model.

2. Modeling of reverse recovery characteristic

2.1. Method

Table 1 shows the definitions of notations used in the figures and equations in this paper. The Ambipolar diffusion constant of i-layer D_{ia} in the table is defined by the following equation.

$$D_{ia} = \frac{2\mu_{ie}\mu_{ih}}{\mu_{ie} + \mu_{ih}}\frac{kT}{q} \tag{2.1.1}$$

Fig. 1 shows a schematic diagram of the pin diode used in this analysis. This diode is set in the circuit as shown in Fig. 2. When the circuit switch shifts from off state to on state, the diode shifts to a reverse recovery mode. Fig. 3 shows the diagram of the reverse recovery waveform, which is divided into five phases [12]. These phases are separated by inflection points of the reverse recovery waveform. Table 2 shows the definitions of the current density J, voltage V, and charge Q at each phase. In addition, Table 3 shows the values of reverse recovery characteristics at the inflection point of the reverse recovery waveform ($t = 0 \sim t_5$).

Conventionally, the reverse recovery characteristics is necessary to calculate the transient phenomena of the electron and hole current distribution in the i-layer [6]. Therefore, it was calculated by the device simulation using a finite element method. In proposed model, the reverse recovery waveform was approximated as a simple shape and divided five phases. Therefore, it is possible to define the time dependent equation of each phase without calculating the transient phenomenon. The sequence of steps followed in the modeling method is as follows.

* Corresponding author.
E-mail address: e1407@mosk.tytlabs.co.jp (Y. Yamashita).

https://doi.org/10.1016/j.sse.2018.02.014
Received 17 November 2017; Received in revised form 23 February 2018; Accepted 26 February 2018
Available online 29 March 2018

Table 1
Definitions of symbols and parameters used for calculation.

Symbol	Definition
N_p	Doping density of p-layer
N_i	Doping density of i-layer
N_n	Doping density of n-layer
d_p	Depth of p-layer
d	Half depth of i-layer
d_n	Depth of n-layer
J	Total current density
J_{rr}	Maximum reverse current density
V	Applied voltage
V_{cc}	Supply voltage
V_s	Surge voltage
Q	Stored charge
Q_{rr}	Reverse recovery charge
W	Width of depletion layer
L_h	Parasitic inductance
$\mathrm{d}J_f/\mathrm{d}t$	Rate of recovery current density decreasing
$\mathrm{d}J_r/\mathrm{d}t$	Rate of recovery current density increasing
$\mathrm{d}J_t/\mathrm{d}t$	Rate of tale current density increasing
$\mathrm{d}V/\mathrm{d}t$	Rate of voltage increasing
η_i	Recombination current density ratio in i-layer
τ_i	Carrier lifetime of i-layer
L_{ia}	Ambipolar diffusion length in i-layer
L_{pe}	Electron diffusion length in p-layer
L_{nh}	Hole diffusion length in n-layer
μ_{ie}	Electron mobility of i-layer
μ_{ih}	Hole mobility of i-layer
μ_{wh}	Hole mobility of depletion layer
D_{ia}	Ambipolar diffusion constant of i-layer
D_{pe}	Electron diffusion constant of p-layer
D_{nh}	Hole diffusion constant of n-layer
$\hat{E}$	Mean electric field in recovery
p	Hole density in recovery
k	Boltzmann constant
T	Temperature
q	Elementary charge

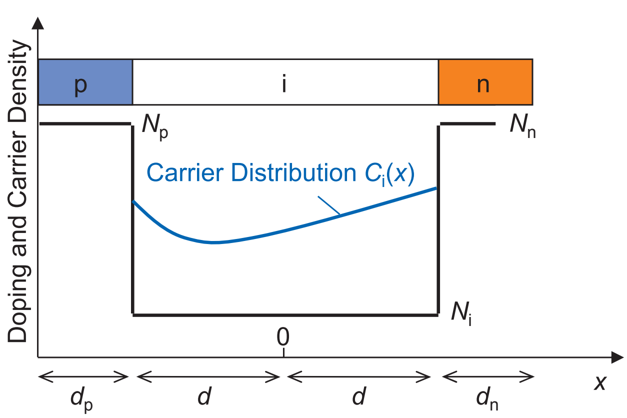

Fig. 1. Schematic diagram of pin diode.

(1) Reverse recovery waveform is divided into five phases [Section 2.1].
(2) Carrier distribution density at $t = 0$ is determined [Section 2.2].
(3) Time dependency equations of current density $J(t)$, voltage $V(t)$ and i-layer charge $Q(t)$ at per phase is derived [Section 2.3].
(4) The relational equation between $J(t)$,$V(t)$ and $Q(t)$ during the reverse recovery is derived [Sections 2.4 and 2.5].
(5) $J(t_1)$ to $J(t_5)$ and $V(t_1)$ to $V(t_5)$ are calculated from the expressions (2)–(4) [Section 2.6].

The relational equation between $J(t)$, $V(t)$ and $Q(t)$ cannot be derived directly. Then, it is derived from the relational equation between $Q(t)$ and the width of depletion layer $W(t)$, and the relational equation between $J(t)$, $V(t)$ and $W(t)$. To confirm the accuracy of this numerical model, we used device simulation. In particular, device simulation of silicon is effective for confirming the accuracy since it can calculate the experiment result accurately.

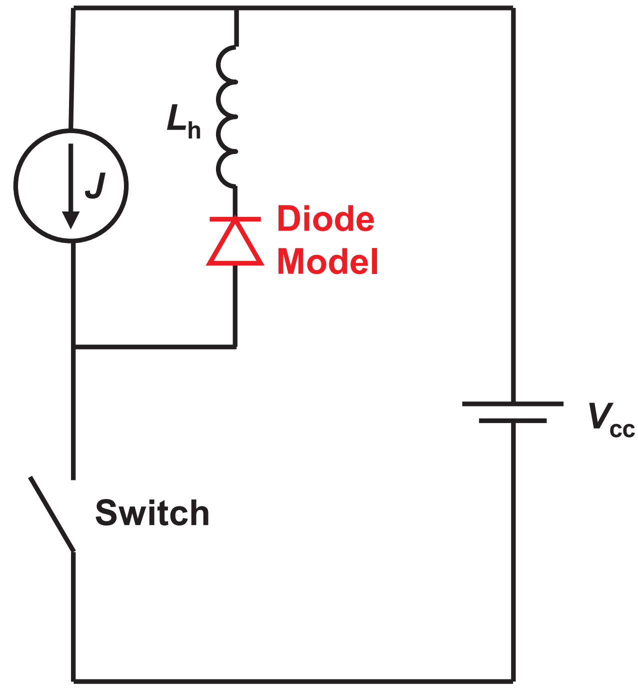

Fig. 2. Circuit diagram of reverse recovery model.

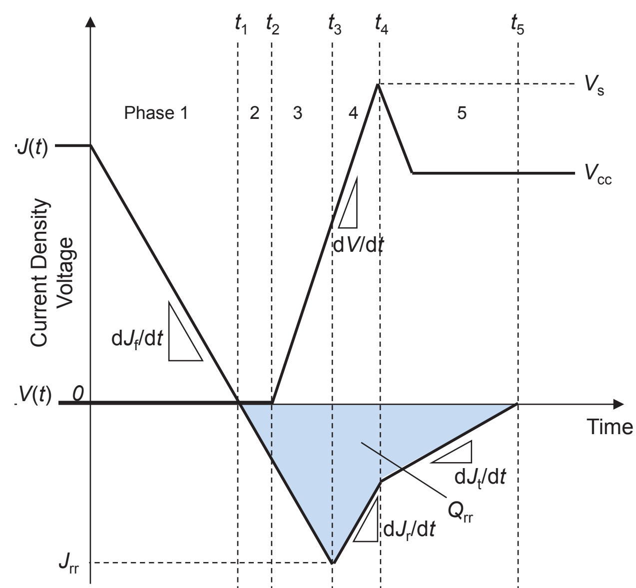

Fig. 3. Schematic diagram of reverse recovery waveform model.

Table 2
Definition of current density, voltage, and charge at each phase.

Phase	$J(t)$	$V(t)$	$Q(t)$
1	$J_{ph1}(t)$	$V_{ph1}(t)$	$Q_{ph1}(t)$
2	$J_{ph2}(t)$	$V_{ph2}(t)$	$Q_{ph2}(t)$
3	$J_{ph3}(t)$	$V_{ph3}(t)$	$Q_{ph3}(t)$
4	$J_{ph4}(t)$	$V_{ph4}(t)$	$Q_{ph4}(t)$
5	$J_{ph5}(t)$	-	$Q_{ph5}(t)$

Table 3
Definition of reverse recovery characteristic values at $0 \sim t_5$.

t	$J(t)$	$V(t)$	$Q(t)$
0	J_0	V_f	Q_0
t_1	0	≒ 0	Q_1
t_2	J_2	≒ 0	Q_2
t_3	J_{rr}	V_3	Q_3
t_4	J_4	V_s	Q_4
t_5	0	V_{cc}	0

2.2. Forward characteristic [4,11,13]

Before calculating the reverse recovery characteristic, it is necessary to calculate the carrier density distribution $C_i(x)$ of the i-layer at time t = 0. When the current density J is flowing, $C_i(x)$ in Fig. 1 can be calculated using the following equation

$$C_{\mathrm{i}}(x) = \frac{J\eta_{\mathrm{i}}\tau_{\mathrm{i}}}{2\mathrm{q}L_{\mathrm{ia}}}\left[\frac{\cosh(x/L_{\mathrm{ia}})}{\sinh(d/L_{\mathrm{ia}})} - B'\frac{\sinh(x/L_{\mathrm{ia}})}{\cosh(d/L_{\mathrm{ia}})}\right]. \tag{2.2.1}$$

B' is a coefficient satisfying the following equation[(Ap)]

$$\frac{h_n(M^2-B')^2}{h_p(M^2+B')^2} = \frac{M(1-B') - \sqrt{M^2(1-B')^2 + 8Ah_n(M^2-B')^2(1-B)}}{M(1+B') - \sqrt{M^2(1+B')^2 + 8Ah_p(M^2+B')^2(1+B)}}, \tag{2.2.2}$$

where

$$B = \frac{\mu_{\mathrm{ie}} - \mu_{\mathrm{ih}}}{\mu_{\mathrm{ie}} + \mu_{\mathrm{ih}}}, \tag{2.2.3}$$

$$M = \frac{\cosh(d/L_{\mathrm{ia}})}{\sinh(d/L_{\mathrm{ia}})}, \tag{2.2.4}$$

$$h_{\mathrm{p}} = \frac{D_{\mathrm{pe}}}{L_{\mathrm{pe}}N_{\mathrm{p}}}\coth\left(\frac{d_{\mathrm{p}}}{L_{\mathrm{pe}}}\right), \tag{2.2.5}$$

$$h_{\mathrm{n}} = \frac{D_{\mathrm{nh}}}{L_{\mathrm{nh}}N_{\mathrm{n}}}\coth\left(\frac{d_{\mathrm{n}}}{L_{\mathrm{nh}}}\right), \tag{2.2.6}$$

$$A = \frac{J\tau_{\mathrm{i}}}{4qD_{\mathrm{ia}}}, \tag{2.2.7}$$

$$\eta_{\mathrm{i}} = \frac{-M(1-B') + \sqrt{M^2(1-B')^2 + 8Ah_n(M^2-B')^2(1-B)}}{4Ah_n(M^2-B')^2}. \tag{2.2.8}$$

The stored charge Q_0 was calculated using the following equation,

$$Q_0 = J\eta_{\mathrm{i}}\tau_{\mathrm{i}}. \tag{2.2.9}$$

The forward voltage V_f is calculated from $C_i(x)$ as

$$V_{\mathrm{f}} = \frac{J}{q(\mu_{\mathrm{ip}} + \mu_{\mathrm{in}})}\cdot\int\frac{1}{C_{\mathrm{i}}(x)}\mathrm{d}x + \frac{kT}{q}\ln\left(\frac{C_{\mathrm{i}}(-d)\cdot C_{\mathrm{i}}(+d)}{n_{\mathrm{i}}^2}\right). \tag{2.2.10}$$

2.3. Time dependence of current density, voltage and charge

In this section, the time dependence equation of the current density J, voltage V, and charge Q in each phase of Fig. 3 is explained.

2.3.1. Phase 1 ($0 < t < t_1$)

This phase is a period until the reverse recovery starts and the current density reaches zero. The current density decreases according to $\mathrm{d}J_f/\mathrm{d}t$from J_0. Assuming that $\mathrm{d}J_f/\mathrm{d}t$has a negative value, the current density during this phase is defined as in Eq. (2.3.1). In addition, the voltage during this phase is almost zero and is defined as in the Eq. (2.3.2).

Current density

$$J_{\mathrm{ph1}}(t) = J_0 + \frac{\mathrm{d}J_{\mathrm{f}}}{\mathrm{d}t}t. \tag{2.3.1}$$

Voltage

$$V_{\mathrm{ph1}}(t) \cong 0. \tag{2.3.2}$$

2.3.2. Phase 2 ($t_1 < t < t_2$)

This phase is a period from the start of the reverse current until the voltage starts to rise. Subsequently, the current density keeps decreasing according to $\mathrm{d}J_f/\mathrm{d}t$. Current density and voltage equations are defined as in Eqs. (2.3.3) and (2.3.4). In this phase, the charge in the i-layer decreases owing to recombination and reverse recovery current, and so a differential equation such as Eq. (2.3.5) is derived. Assuming that the charge at t_1 is Q_1, the solution is derived as shown in Eq. (2.3.6).

Current density

$$J_{\mathrm{ph2}}(t) = \frac{\mathrm{d}J_{\mathrm{f}}}{\mathrm{d}t}(t-t_1). \tag{2.3.3}$$

Voltage

$$V_{\mathrm{ph2}}(t) \cong 0. \tag{2.3.4}$$

Charge

$$\frac{\mathrm{d}Q_{\mathrm{ph2}}(t-t_1)}{\mathrm{d}t} = -\frac{Q_{\mathrm{ph2}}(t-t_1)}{\tau_{\mathrm{i}}} + \frac{\mathrm{d}J_{\mathrm{f}}}{\mathrm{d}t}(t-t_1). \tag{2.3.5}$$

$$Q_{\mathrm{ph2}}(t) = \tau_{\mathrm{i}}^2\frac{\mathrm{d}J_{\mathrm{f}}}{\mathrm{d}t}(e^{-(t-t_1)/\tau_{\mathrm{i}}}-1) + \frac{\mathrm{d}J_{\mathrm{f}}}{\mathrm{d}t}\tau_{\mathrm{i}}(t-t_1) + Q_1e^{-(t-t_1)/\tau_{\mathrm{i}}}. \tag{2.3.6}$$

2.3.3. Phase 3 ($t_2 < t < t_3$)

This phase is a period until the voltage starts to rise and the current density reaches the maximum value J_{rr}. The current density decreases according to $\mathrm{d}J_f/\mathrm{d}t$. In this phase, the current density is defined by Eq. (2.3.7). In addition, since the voltage starts to rise according to $\mathrm{d}V/\mathrm{d}t$, it is defined as in the Eq. (2.3.8). The amount of charge in the i-layer decreases owing to recombination and reverse recovery current, and so a differential equation such as Eq. (2.3.9) is derived. Assuming that the charge at t_2 is Q_2, a solution is calculated using Eq. (2.3.10).

Current density

$$J_{\mathrm{ph3}}(t) = \frac{\mathrm{d}J_{\mathrm{f}}}{\mathrm{d}t}(t-t_1). \tag{2.3.7}$$

Voltage

$$V_{\mathrm{ph3}}(t) = \frac{\mathrm{d}V}{\mathrm{d}t}(t-t_2). \tag{2.3.8}$$

Charge

$$\frac{\mathrm{d}Q_{\mathrm{ph3}}(t-t_2)}{\mathrm{d}t} = -\frac{Q_{\mathrm{ph3}}(t-t_2)}{\tau_{\mathrm{i}}} + \frac{\mathrm{d}J_{\mathrm{f}}}{\mathrm{d}t}(t-t_2). \tag{2.3.9}$$

$$Q_{\mathrm{ph3}}(t) = \tau_{\mathrm{i}}^2\frac{\mathrm{d}J_{\mathrm{f}}}{\mathrm{d}t}(e^{-(t-t_2)/\tau_{\mathrm{i}}}-1) + \frac{\mathrm{d}J_{\mathrm{f}}}{\mathrm{d}t}\tau_{\mathrm{i}}(t-t_2) + Q_2e^{-(t-t_2)/\tau_{\mathrm{i}}}. \tag{2.3.10}$$

2.3.4. Phase 4 ($t_3 < t < t_4$)

This phase is a period in which the current density reverses and starts to rise until the voltage reaches a maximum value of V_s. Since the current density rises according to $\mathrm{d}J_r/\mathrm{d}t$ from J_{rr}, the current density is defined as in Eq. (2.3.11). Since the voltage rises according to $\mathrm{d}V/\mathrm{d}t$, similar to Phase 3, it is defined as in Eq. (2.3.12). In addition, since the charge decreases owing to recombination and reverse recovery current, a differential equation such as Eq. (2.3.13) was obtained. When the charge amount at t_3 is Q_3, then the solution is calculated using Eq. (2.3.14).

Current density

$$J_{ph4}(t) = J_{rr} + \frac{dJ_r}{dt}(t-t_3). \tag{2.3.11}$$

Voltage

$$V_{ph4}(t) = \frac{dV}{dt}(t-t_2). \tag{2.3.12}$$

Charge

$$\frac{dQ_{ph4}(t-t_3)}{dt} = -\frac{Q_{ph4}(t-t_3)}{\tau_i} - \left[-J_{rr} - \frac{dJ_r}{dt}(t-t_3)\right]. \tag{2.3.13}$$

$$Q_{ph4}(t) = \left(\tau_i^2\frac{dJ_r}{dt} - \tau_i J_{rr}\right)(e^{-(t-t_3)/\tau_i} - 1) + \frac{dJ_r}{dt}\tau_i(t-t_3) + Q_3 e^{-(t-t_3)/\tau_i}. \tag{2.3.14}$$

2.3.5. Phase 5 ($t_4 < t < t_5$)

This phase is a period until the current density reaches zero after the voltage reaches V_s. The current density rises with dJ_r/dt. The current density during this phase is given by Eq. (2.3.15), where J_4 is the current density at t_4. In addition, since the charge decreases owing to recombination and reverse recovery current, a differential equation such as Eq. (2.3.16) is derived. Assuming that the charge at t_4 is Q_4, a solution like Eq. (2.3.17) is obtained.

Current density

$$J_{ph5}(t) = J_4 + \frac{dJ_t}{dt}(t-t_4). \tag{2.3.15}$$

Charge

$$\frac{dQ_{ph5}(t-t_4)}{dt} = -\frac{Q_{ph5}(t-t_4)}{\tau_i} - \left[-J_4 - \frac{dJ_t}{dt}(t-t_4)\right]. \tag{2.3.16}$$

$$Q_{ph5}(t) = \left(\tau_i^2\frac{dJ_t}{dt} - \tau_i J_4\right)(e^{-(t-t_4)/\tau_i} - 1) + \frac{dJ_t}{dt}\tau_i(t-t_4) + Q_4 e^{-(t-t_4)/\tau_i}. \tag{2.3.17}$$

2.4. Relationship between width of depletion layer and charge

In order to obtain a relational equation between the depletion layer width W and the charge Q, a carrier distribution is calculated during reverse recovery. Carriers in the i-layer under reverse recovery are swept out as reverse recovery currents owing to diffusion and drift, and disappear by recombination.

First, consider the change in carrier distribution due to diffusion and recombination. Focusing on the carrier distribution density $C_i(x_d)$ in a minute region dx_d of depth x_d, the area density $C_{id}(x_d)$ of the carrier at the depth x_d is

$$C_{id}(x_d) = C_i(x_d)dx_d. \tag{2.4.1}$$

The time dependence of this charge at this time is expressed by the following equation [14].

$$C_{id}(x,t) = \frac{C_i(x_d)dx_d}{\sqrt{4\pi D_{ia}t}}\exp\left\{-\frac{(x-x_d)^2}{4D_{ia}t} - \frac{t}{\tau_i}\right\}, \tag{2.4.2}$$

By integrating x_d in this equation from depth -d to d, the carrier distribution $C_i(x,t)$ in diffusion and recombination is calculated as follows.

$$\begin{aligned} C_i(x,t) &= \int_{-d}^{+d}\frac{C_i(x_d)}{\sqrt{4\pi D_{ia}t}}\exp\left\{-\frac{(x-x_d)^2}{4D_{ia}t} - \frac{t}{\tau_i}\right\}dx_d \\ &= \frac{J\eta_i\tau_i}{2qL_{ia}}\exp\left(-\frac{x}{L_{ia}}\right)\left(B'\frac{1}{\cosh(d/L_{ia})} + \frac{1}{\sinh(d/L_{ia})}\right)\cdot \\ &\left[erf\left(\frac{(d-x)}{2\sqrt{D_{ia}t}} + \sqrt{\frac{t}{\tau_i}}\right) - erf\left(\frac{(-d-x)}{2\sqrt{D_{ia}t}} + \sqrt{\frac{t}{\tau_i}}\right)\right] \\ &- \frac{J\eta_i\tau_i}{2qL_{ia}}\exp\left(\frac{x}{L_{ia}}\right)\left(\frac{1}{\sinh(d/L_{ia})} - B'\frac{1}{\cosh(d/L_{ia})}\right)\cdot \\ &\left[erf\left(\frac{(x+d)}{2\sqrt{D_{ia}t}} + \sqrt{\frac{t}{\tau_i}}\right) - erf\left(\frac{(x-d)}{2\sqrt{D_{ia}t}} + \sqrt{\frac{t}{\tau_i}}\right)\right]. \end{aligned} \tag{2.4.3}$$

Next, the case where the depletion layer expands, and carriers are swept out during reverse recovery is considered. It is assumed that the depletion layer extends from the p/i interface. When the width of the depletion layer is W, the charge is obtained by integrating the equation from $-d + W$ to $+d$. The charge during the reverse recovery period is calculated as shown in the following equation. This equation corresponds to the relational equation between W and Q.

$$\begin{aligned} \int_{-d+W}^{+d} C_i(x,t)dx = {} & \frac{J\eta_i\tau_i}{2q}\left(B'\frac{1}{\cosh(d/L_{ia})} + \frac{1}{\sinh(d/L_{ia})}\right)\left[-\exp\left(-\frac{d}{L_{ia}}\right)erf\left(\sqrt{\frac{t}{\tau_i}}\right)\right. \\ & + \exp\left(-\frac{D_{ia}t - dL_{ia}}{L_{ia}^2}\right)erf\left(-\frac{W}{2\sqrt{D_{ia}t}}\right) \\ & - \exp\left(\frac{d-W}{L_{ia}}\right)erf\left(-\frac{W}{2\sqrt{D_{ia}t}} + \sqrt{\frac{t}{\tau_i}}\right) \\ & - \exp\left(-\frac{D_{ia}t - dL_{ia}}{L_{ia}^2}\right)erf\left(-\frac{d}{\sqrt{D_{ia}t}}\right) \\ & + \exp\left(-\frac{d}{L_{ia}}\right)erf\left(-\frac{d}{\sqrt{D_{ia}t}} + \sqrt{\frac{t}{\tau_i}}\right) \\ & - \exp\left(-\frac{D_{ia}t + dL_{ia}}{L_{ia}^2}\right)erf\left(\frac{(2d-W)}{2\sqrt{D_{ia}t}}\right) \\ & \left. + \exp\left(\frac{d-W}{L_{ia}}\right)erf\left(\frac{(2d-W)}{2\sqrt{D_{ia}t}} + \sqrt{\frac{t}{\tau_i}}\right)\right] \\ & + \frac{J\eta_i\tau_i}{2q}\left(\frac{1}{\sinh(d/L_{ia})} - B'\frac{1}{\cosh(d/L_{ia})}\right)[-\exp\left(\frac{d}{L_{ia}}\right)erf\left(\sqrt{\frac{t}{\tau_i}}\right) \\ & + \exp\left(-\frac{D_{ia}t + dL_{ia}}{L_{ia}^2}\right)erf\left(\frac{W}{2\sqrt{D_{ia}t}}\right) \\ & - \exp\left(\frac{-d+W}{L_{ia}}\right)erf\left(\frac{W}{2\sqrt{D_{ia}t}} + \sqrt{\frac{t}{\tau_i}}\right) \\ & - \exp\left(-\frac{D_{ia}t + dL_{ia}}{L_{ia}^2}\right)erf\left(\frac{d}{\sqrt{D_{ia}t}}\right) \\ & + \exp\left(\frac{d}{L_{ia}}\right)erf\left(\frac{d}{\sqrt{D_{ia}t}} + \sqrt{\frac{t}{\tau_i}}\right) \\ & - \exp\left(-\frac{D_{ia}t - dL_{ia}}{L_{ia}^2}\right)erf\left(\frac{(-2d+W)}{2\sqrt{D_{ia}t}}\right) \\ & + \exp\left(\frac{-d+W}{L_{ia}}\right)erf\left(\frac{(-2d+W)}{2\sqrt{D_{ia}t}} + \sqrt{\frac{t}{\tau_i}}\right), \end{aligned} \tag{2.4.4}$$

2.5. Relationship between current density, voltage and width of depletion layer

In this section, the relationship between the current density J, voltage V, and depletion layer width W is calculated. Fig. 4 shows the pin diode diagram with the expansion of the depletion layer during reverse recovery. We assume that all the voltage is applied to the depletion layer region during reverse recovery, i.e.,

$$V(t) = \frac{1}{2}E_0 W(t), \tag{2.5.1}$$

Furthermore, assuming that the small hole density remaining in the

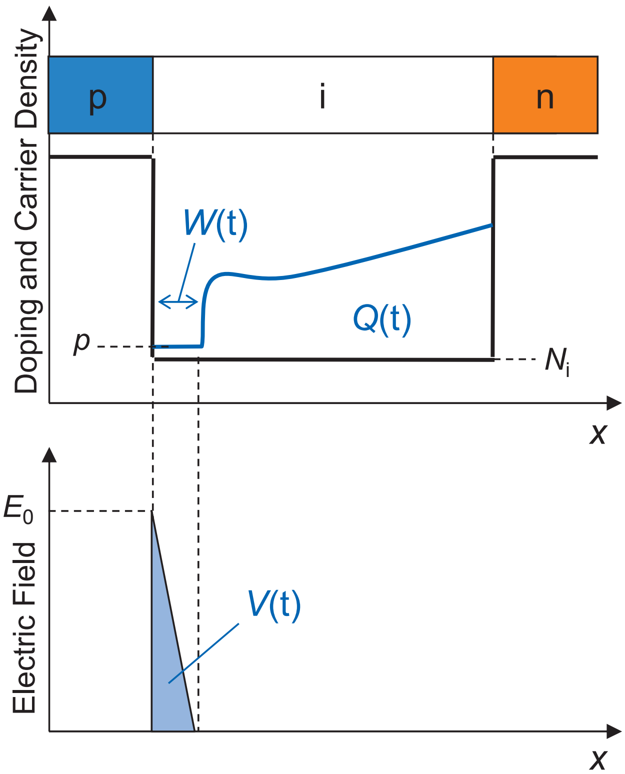

Fig. 4. Schematic diagram of pin diode during reverse recovery period.

depletion layer region is p, the following equation is established from the Poisson equation.

$$\frac{E_0}{W(t)}\cdot\frac{\varepsilon}{q} = p + N_i, \tag{2.5.2}$$

Substituting Eq. (2.5.2) into Eq. (2.5.1) to erase electric field E, following equation is derived,

$$\frac{2V(t)}{W(t)^2}\cdot\frac{\varepsilon}{q} = p + N_i. \tag{2.5.3}$$

During reverse recovery, only the hole current flows in the depletion layer. Hence, in the depletion layer, the total current density $J(t)$ can be represented only by the drift current of the holes. $J(t)$ is expressed as follows with the hole mobility of depletion layer μ_{wh} and the mean electric field of depletion layer $\widehat{E}$,

$$J(t) = q\mu_{\mathrm{wh}}p\widehat{E}. \tag{2.5.4}$$

$$\widehat{E} = \frac{V(t)}{W(t)}. \tag{2.5.5}$$

When p and $\widehat{E}$ are eliminated using Eqs. (2.5.3)–(2.5.5), a relational equation of current density $J(t)$, voltage $V(t)$, and depletion layer width $W(t)$ during reverse recovery is obtained as shown in the following equation.

$$J(t) = \frac{V(t)\mu_{\mathrm{wh}}(2\varepsilon V(t) - qN_{\mathrm{i}}W(t)^2)}{W(t)^3}. \tag{2.5.6}$$

The comparison between $J(t)$ from Eq. (2.5.6) and device simulation is shown in the Fig. 5. $W(t)$ of Eq. (2.5.6) are calculated from device simulation. The tendencies of "Eq. (2.5.6)" and "Simulation" are in good agreement, and $J(t)$ can be approximated by $W(t)$ and $V(t)$.

2.6. Calculation

In this section, J_1 to J_4, V_3 to V_s, and Q_1 to Q_4 were derived by using

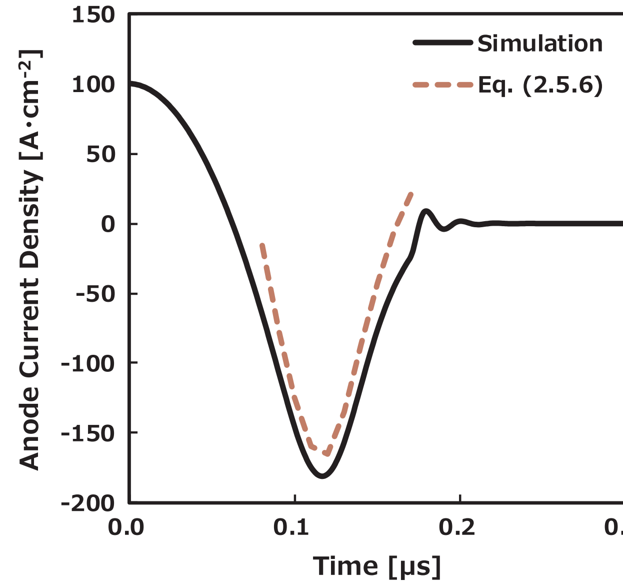

Fig. 5. Comparison between current waveform directly calculated from simulation and calculated using Eq. (2.5.6), 2d = 140 μm, $N_p = N_n = 10^{16}\,\mathrm{cm}^{-3}$, $N_i = 5 \times 10^{13}\,\mathrm{cm}^{-3}$, T = 25 °C and $\tau_i = 10\,\mu\mathrm{s}$.

the time change equations in Section 2.3, and the relational equations in Sections 2.4 and 2.5.

2.6.1. When $t = t_1$

t_1 was calculated from Eq. (2.3.1). When $W = 0$ in Eq. (2.4.4), Q_1 was derived as follows,

$$t_1 = -J_0/\frac{\mathrm{d}J_{\mathrm{f}}}{\mathrm{d}t}, \tag{2.6.1}$$

$$Q_1 = \int_{-d}^{+d} C_{\mathrm{i}}(x,t_1)dx. \tag{2.6.2}$$

2.6.2. When $t = t_2$

From Eqs. (2.3.6) and (2.4.4), the following equation was established,

$$\int_{-d}^{+d} C_{\mathrm{i}}(x,t_2)dx = Q_2. \tag{2.6.3}$$

By obtaining t_2 satisfying the Eq. (2.6.3), J_2 and Q_2 were calculated as follows,

$$J_2 = \frac{\mathrm{d}J_{\mathrm{f}}}{\mathrm{d}t}(t_2 - t_1), \tag{2.6.4}$$

$$Q_2 = \tau_{\mathrm{i}}^2\frac{\mathrm{d}J_{\mathrm{f}}}{\mathrm{d}t}(e^{-(t_2-t_1)/\tau_{\mathrm{i}}} - 1) + \frac{\mathrm{d}J_{\mathrm{f}}}{\mathrm{d}t}\tau_{\mathrm{i}}(t_2 - t_1) + Q_1 e^{-(t_2-t_1)/\tau_{\mathrm{i}}}. \tag{2.6.5}$$

2.6.3. When $t = t_3$

From Eqs. (2.3.10) and (2.4.4), the following equation was derived,

$$\int_{-d+W_3}^{+d} C_{\mathrm{i}}(x,t_3)dx = Q_3. \tag{2.6.6}$$

Further, from Eqs. (2.3.7), (2.3.8) and (2.5.6), the following equation was derived,

$$-\frac{\mathrm{d}J_{\mathrm{f}}}{\mathrm{d}t}(t_3 - t_2) = \frac{2\varepsilon\mu_{\mathrm{ip}}}{W_3^3}\left(\frac{\mathrm{d}V}{\mathrm{d}t}(t_3 - t_2)\right)^2 - \frac{q\mu_{\mathrm{ip}}N_{\mathrm{i}}}{W_3}\left(\frac{\mathrm{d}V}{\mathrm{d}t}(t_3 - t_2)\right). \tag{2.6.7}$$

By obtaining W_3 and t_3 satisfying Eqs. (2.6.6) and (2.6.7), J_{rr}, V_3, Q_3 were calculated as follows,

$$J_{\mathrm{rr}} = \frac{\mathrm{d}J_{\mathrm{f}}}{\mathrm{d}t}(t_3 - t_1), \tag{2.6.8}$$

$$V_3 = \frac{dV}{dt}(t-t_2), \tag{2.6.9}$$

$$Q_3 = \tau_i^2\frac{dJ_f}{dt}(e^{-(t_3-t_2)/\tau_i}-1) + \frac{dJ_f}{dt}\tau_i(t_3-t_2) + Q_2e^{-(t_3-t_2)/\tau_i}. \tag{2.6.10}$$

2.6.4. When $t = t_4$

From Eqs. (2.3.14) and (2.4.4), the following equation was derived,

$$\int_{-d+W_4}^{+d} C_i(x,t_4)dx = Q_4. \tag{2.6.11}$$

From Eqs. (2.3.11), (2.3.12) and (2.5.6), the following equation was derived,

$$-J_{rr}-\frac{dJ_r}{dt}(t_4-t_3) = \frac{2\varepsilon\mu_{ip}}{W_4^3}\left(\frac{dV}{dt}(t_4-t_2)\right)^2-\frac{q\mu_{ip}N_i}{W_4}\left(\frac{dV}{dt}(t_4-t_2)\right). \tag{2.6.12}$$

Further, the surge voltage V_s has the following equation from the parasitic inductances L_h and dJ_r/dt in Fig. 3,

$$V_s-V_{cc} = L_h\frac{dJ_r}{dt}. \tag{2.6.13}$$

From Eqs. (2.3.11) and (2.6.13) the following expression can be obtained

$$\frac{dV}{dt}(t_4-t_2)-V_{cc} = L_h\frac{dJ_r}{dt}. \tag{2.6.14}$$

By obtaining t_4 and dJ_r/dt satisfying Eqs. (2.6.11), (2.6.12) and (2.6.14), J_4, V_s, Q_4 was calculated,

$$J_4 = J_{rr} + \frac{dJ_r}{dt}(t_4-t_3), \tag{2.6.15}$$

$$V_s = \frac{dV}{dt}(t_4-t_2), \tag{2.6.16}$$

$$Q_4 = \left(\tau_i^2\frac{dJ_r}{dt}-\tau_iJ_{rr}\right)(e^{-(t_4-t_3)/\tau_i}-1) + \frac{dJ_r}{dt}\tau_i(t_4-t_3) + Q_3e^{-(t_4-t_3)/\tau_i}. \tag{2.6.17}$$

2.6.5. When $t = t_5$

Since J and Q become 0, the following equations are established from Eqs. (2.3.15) and (2.3.17),

$$0 = \left(\tau_i^2\frac{dJ_t}{dt}-\tau_iJ_4\right)(e^{-(t_5-t_4)/\tau_i}-1) + \frac{dJ_t}{dt}\tau_i(t_5-t_4) + Q_4e^{-(t_5-t_4)/\tau_i}, \tag{2.6.18}$$

$$0 = -J_4 + \frac{dJ_t}{dt}(t_5-t_4). \tag{2.6.19}$$

t_5 and dJ_t/dt are calculated such that they satisfy Eqs. (2.6.18) and (2.6.19).

3. Calculation result

It is necessary to solve the equations of this model using numerical analysis such as Newton's method. Then, in this paper, we created an algorithm to calculate the following by VBA.

3.1. Forward characteristic

The structural parameters shown in Fig. 1(a) are determined and $C_i(x)$,V_f are calculated from Eqs. (2.2.1) and (2.2.10).

3.2. Flow of calculating t_1

t_1 and Q_1 were calculated directly using Eq. (2.6.1).

3.3. Flow of calculating t_2

First, the initial value of t_2 is determined then Q_2 is defined from Eq. (2.6.5) by substituting t_2. When Q_2 is determined, the right side of Eq. (2.6.3) can be defined. Finally, t_2 that satisfies the Eq. (2.6.3) is searched using the Newton's method.

3.4. Flow of calculating t_3

First, the initial value of t_3 is determined then the left side of Eq. (2.6.7) and Q_3 of Eq. (2.6.10) are calculated by substituting t_3. Second, W_3 is calculated by Q_3 using Eq. (2.6.6). Third, the right side of Eq. (2.6.7) is calculated by W_3. Finally, t_3 that satisfies Eq. (2.6.7) is searched using the Newton's method.

3.5. Flow of calculating t_4

First, the initial value of t_4 is determined then the left side of Eq. (2.6.12) and dJ_r/dt of Eq. (2.6.14) are calculated by substituting t_4. Second, Q_4 is calculated by dJ_r/dt using Eq. (2.6.17). W_4 is calculated by Q_3 using Eq. (2.6.11). Third, the right side of Eq. (2.6.12) is calculated by W_4. Finally, t_4 that satisfies Eq. (2.6.12) is searched using the Newton's method.

3.6. Flow of calculating t_5

First, the initial value of t_5 is determined then dJ_t/dt of Eq. (2.6.19) is calculated by substituting t_5. Second, the right side of Eq. (2.6.18) is calculated by dJ_t/dt. Finally, t_5 that satisfies Eq. (2.6.18) is searched using the Newton's method.

In order to verify the validity and the accuracy of the numerical model, the calculation result from the model is verified through the device simulation result. For each structure parameter, the i-layer thickness was $2d = 140\,\mu$m, p-layer and n-layer density (N_p, N_n) was $10^{16}\,\text{cm}^{-3}$, i-layer density was $N_i = 5\times10^{13}\,\text{cm}^{-3}$, temperature was $T = 25\,°$C, and carrier lifetime was $\tau_i = 10\,\mu$s. The circuit parameters were $L_h = 100\,$nH and turn off time of the switch is $10\,\mu$s. The simulation, Sentaurus of Synopsys, was executed using CPU: Xeon, RAM: 96 GB, OS: Linux calculation server. The calculation time was approximately 60 s per condition. The numerical model was executed using VBA (Visual Basic for Applications) with CPU: Corei5, RAM: 8.00 GB, OS: Windows 7 (64 bit) PC. The calculation time was approximately 0.05 s per condition.

Fig. 6 shows an example comparison of reverse recovery waveform obtained from numerical model ("Equation") and device simulation ("Simulation"). As shown in the figure, the waveform is close to the simulation result. Figs. 7–9 show the dependency of the current density J_0, the supply voltage V_{cc} and temperature on reverse recovery properties, such as the maximum reverse recovery current density J_{rr}, reverse recovery charge Q_{rr} and surge voltage V_s. The result from equations was obtained as a continuous solution. In addition, the lines of the equations show a similar tendency to the point of the simulation. In particular, the current density dependence of the surge voltage (Fig. 8(c)) coincided with the trend that it shows the maximum value on the low current region. This is also match with our previous experimental results [15].

However, the line of the equation deviates from the result of the simulation tendency in the high voltage region (the solid line in Figs. 8(b) and (c) and 9(c)). Fig. 10 shows waveform comparison at $V_{cc} = 800\,$V. In this case, the oscillation phenomenon occurred in the simulation, and it greatly diverged from the numerical model that does not assume oscillation. When an oscillation phenomenon occurs, a depletion layer spreads from the i/n interface during reverse recovery [12]. Since this model does not assume the development of the depletion layer from other than the p/i interface, the error expanded.

Therefore, this model is applicable under the following conditions.

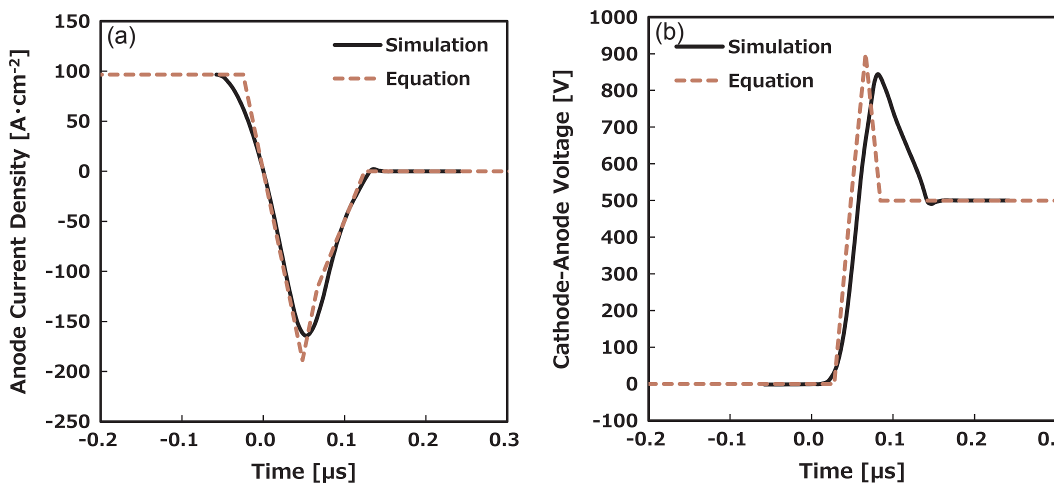

Fig. 6. Comparison of reverse recovery waveform numerical model and device simulation (J_0 = 100 A cm^{-2}, V_{cc} = 500 V, T = 298 K) (a) current density waveform and (b) voltage waveform.

1. The doping concentration of p, i and n-layer are constant.
2. The lifetime in the i-layer is constant.
3. The depletion layer during reverse recovery only develops from the p/i interface. (Double side penetration phenomenon cannot be calculated.)
4. Dynamic avalanche cannot be calculated.

Conditions 3 and 4 require as shown in the following equation, the damping factor $\zeta < 0.1$ and $J_4 < J_{soa}^{12)}$.

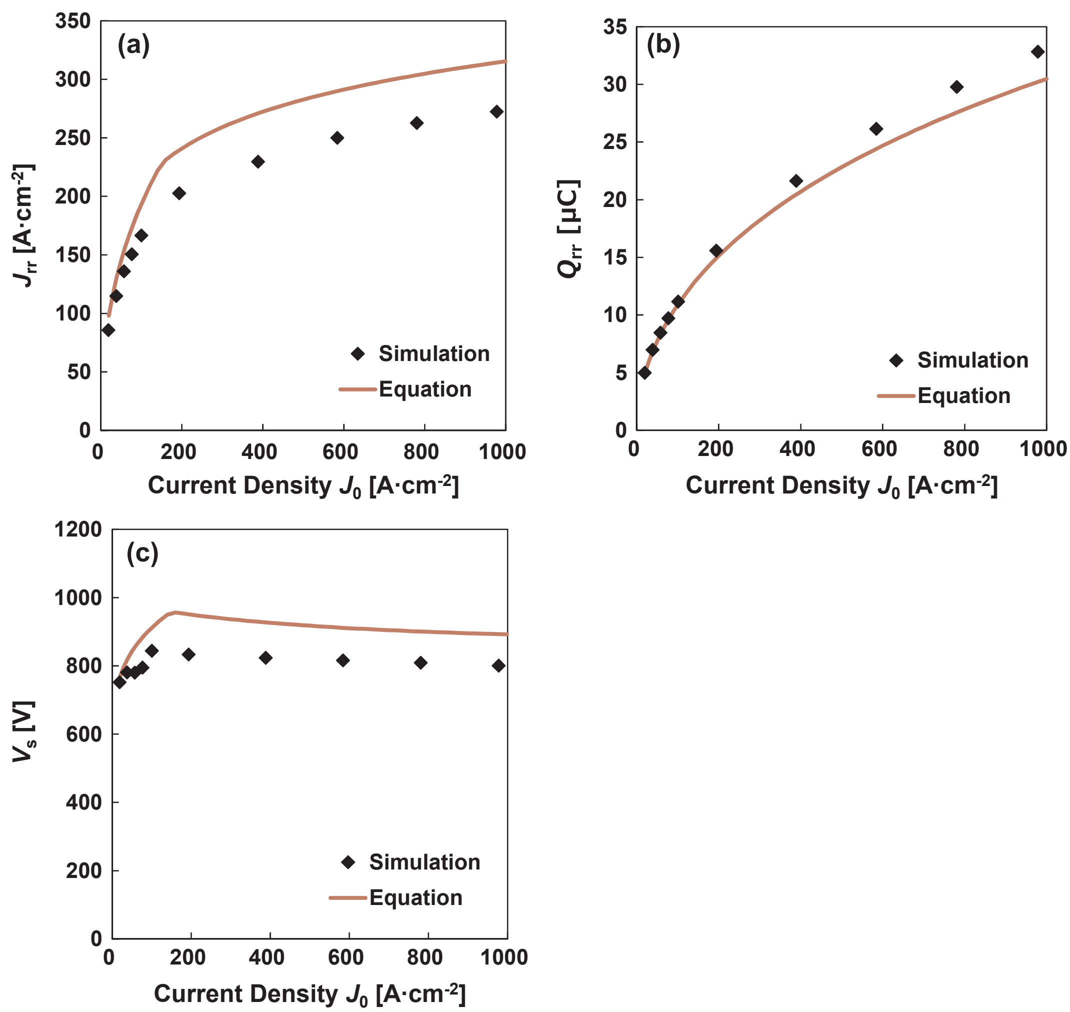

Fig. 7. Dependency of current density J_0 on (a) maximum reverse current density J_{rr}, (b) reverse recovery charge Q_{rr} and (c) surge voltage V_s, calculated from numerical mode and device simulation (V_{cc} = 500 V, T = 298 K).

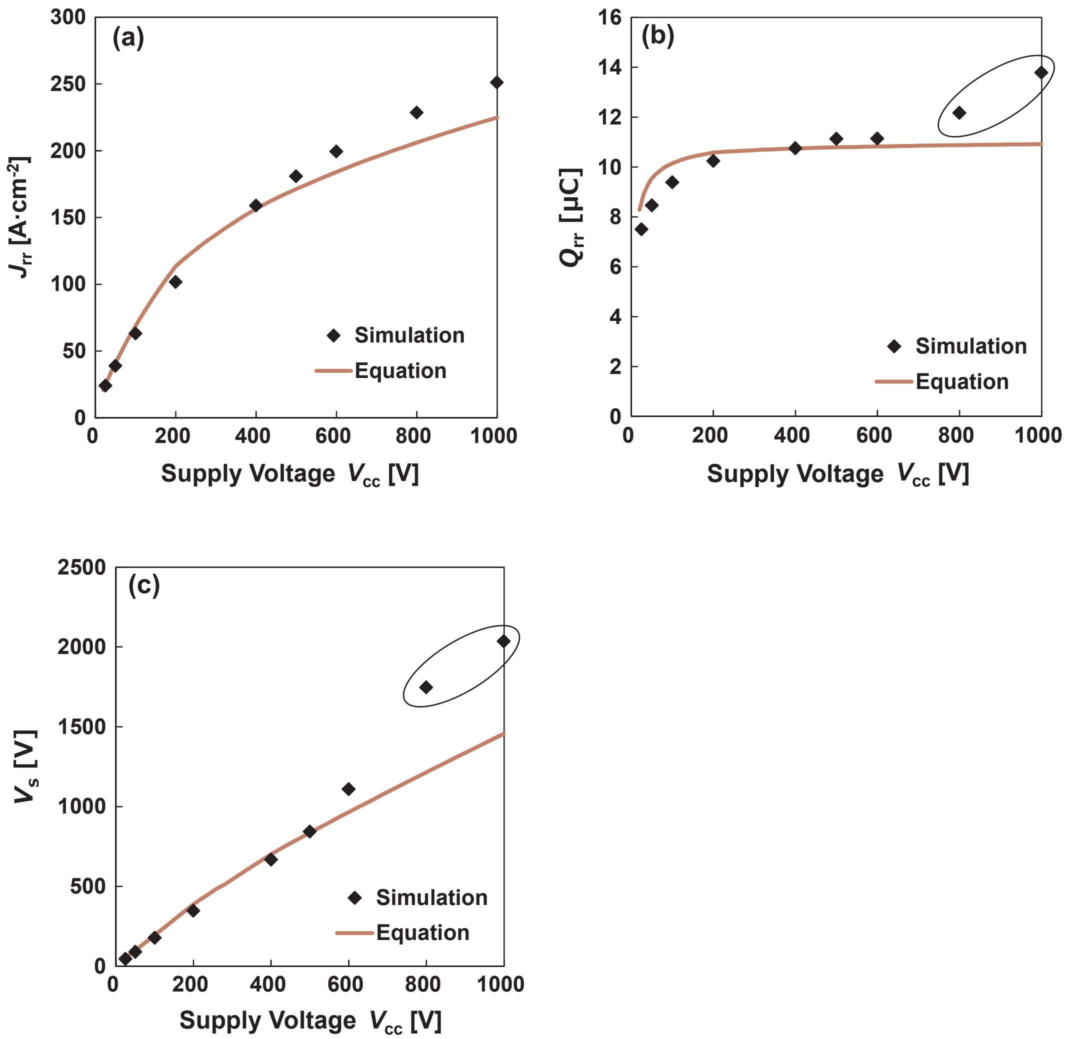

Fig. 8. Dependency of supplied voltage V_{cc} on (a) maximum reverse current density J_{rr}, (b) reverse recovery charge Q_{rr} and (c) surge voltage V_s, calculated from numerical mode and device simulation (J_0 = 100 A cm^{-2}, T = 298 K).

$$\zeta \approx \frac{1}{2}\sqrt{\frac{C_{\mathrm{D}}}{L_{\mathrm{h}}}} < 0.1 \tag{3.1}$$

$$J_4 < J_{\mathrm{SOA}} = 10^7 \times qN_{\mathrm{i}}\left[\frac{V_{\mathrm{bd}}}{V(t_4)} - 1\right] \tag{3.2}$$

where C_D is capacitance of i-layer, V_{bd} is breakdown voltage and,

$$C_{\mathrm{D}} = \frac{\mathrm{d}Q}{\mathrm{d}V} = \frac{\Delta Q_4}{\Delta V_4} \tag{3.3}$$

$$\Delta Q_4 = \int_{-d+W_4'}^{+d} C_{\mathrm{i}}(x,t_4)dx - \int_{-d+W_4}^{+d} C_{\mathrm{i}}(x,t_4)dx \tag{3.4}$$

$$\Delta V_4 = V_4' - V_4 \tag{3.5}$$

W_4' and V_4' are calculated using the Newton's method from the following equation.

$$J_4 = \frac{V_4'\mu_{\mathrm{wh}}(2\varepsilon V_4' - qN_{\mathrm{i}}W_4'^2)}{W_4'^3} \tag{3.6}$$

4. Conclusion

We proposed a new numerical reverse recovery model of silicon pin diode as a function of structural parameters and circuit parameters. This is the first model to calculate the reverse recovery characteristics using the numerical equations without adjusted by fitting equations and fitting parameters. In this model, the reverse recovery waveform was approximated as a simple shape and divided five phases. Therefore, it is possible to define the time dependent equation of each phase without calculating the transient phenomenon of the electron and hole current distribution. This model was able to calculate the voltage and current dependency similar to device simulation as a continuous solution, and it can calculate more than 1000 times faster to get consequence per condition. This model could be useful for device development as a quick calculation. And it could be also useful to academical and educational understanding the behavior of the electrical characteristics.

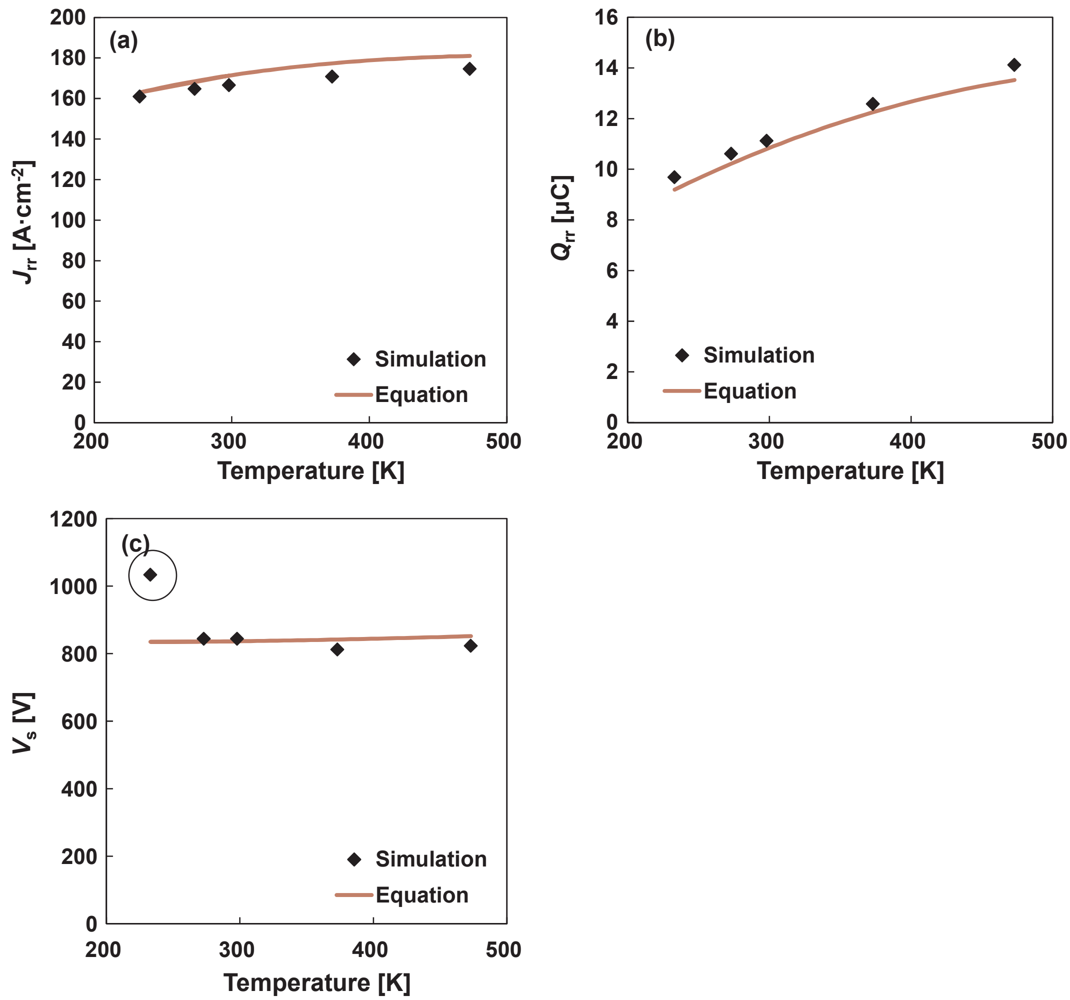

Fig. 9. Dependency of Temperature on (a) maximum reverse current density J_{rr}, (b) reverse recovery charge Q_{rr} and (c) surge voltage V_s, calculated from numerical mode and device simulation (J_0 = 100 A cm^{-2}, V_{cc} = 500 V).

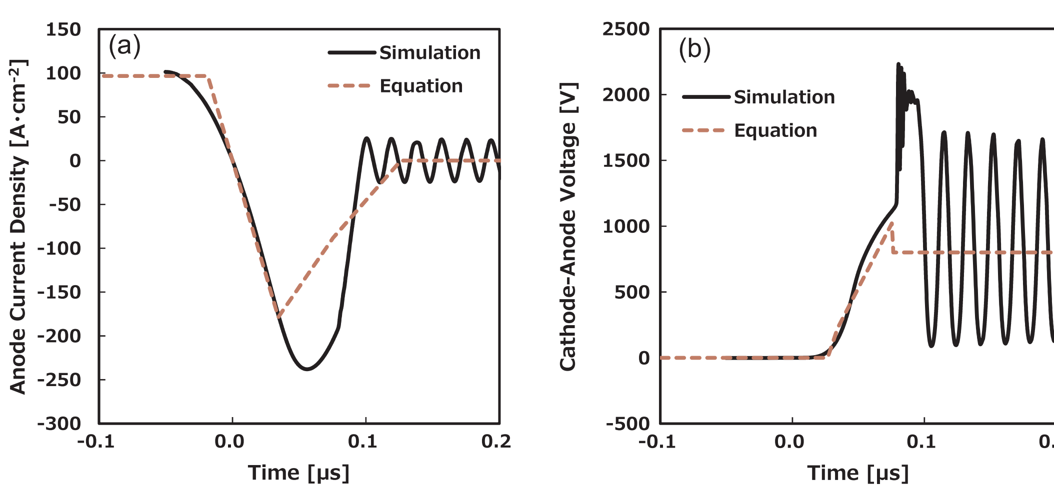

Fig. 10. Comparison of reverse recovery waveform numerical model and device simulation (V_{cc} = 800 V), (a) current density waveform and (b) voltage waveform.

Appendix A

B' can be calculated from the ratio of recombination current and diffusion current as the following equation.

$$B' = \frac{1}{\eta_{\mathrm{i}}}(B + \eta_{\mathrm{nh}} - \eta_{\mathrm{pe}}). \tag{A.1}$$

B is expressed by the ratio of μ_{ie} and μ_{ih}.

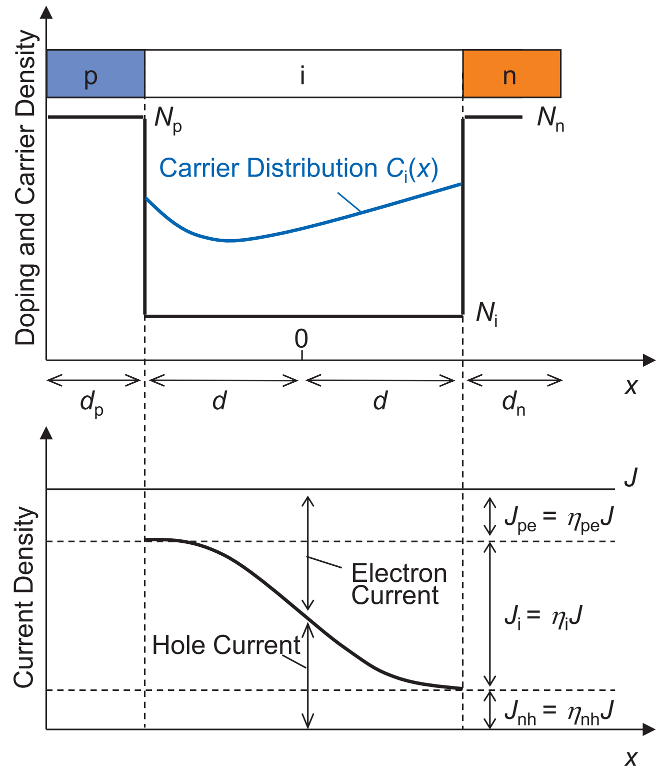

Fig. A1. Schematic diagram of current density distribution.

$$B = \frac{\mu_{ie} - \mu_{ih}}{\mu_{ie} + \mu_{ih}} \tag{2.2.3}$$

The electron current J_{pe} at the p/i interface and the hole current J_{nh} at the i/n interface are expressed by the following equations.

$$J_{pe} = J\eta_{pe} = q\frac{D_{pe}}{L_{pe}}\coth\left(\frac{d_p}{L_{pe}}\right)\frac{C_i(-d)^2}{N_p} \tag{A.2}$$

$$J_{nh} = J\eta_{nh} = q\frac{D_{nh}}{L_{nh}}\coth\left(\frac{d_n}{L_{nh}}\right)\frac{C_i(+d)^2}{N_n} \tag{A.3}$$

The following equation is obtained from Fig. A1.

$$\eta_{pe} + \eta_i + \eta_{nh} = 1 \tag{A.4}$$

B' is obtained from the simultaneous equations of Eqs. (A.1)–(A.4).

First, by substituting d into Eq. (2.2.1), we obtain,

$$C_i(-d) = \frac{J\eta_i\tau_i}{2qL_{ia}M}(M^2 + B') \tag{A.5}$$

$$C_i(+d) = \frac{J\eta_i\tau_i}{2qL_{ia}M}(M^2 - B') \tag{A.6}$$

$$M = \frac{\cosh(d/L_{ia})}{\sinh(d/L_{ia})} \tag{A.7}$$

By substituting Eq. (A.5) into (A.2) and Eq. (A.6) into (A.3) and solved with η_{pe} and η_{nh}, we obtain,

$$\eta_{pe} = \frac{Ah_p}{M^2}\eta_i^2(M^2 + B')^2 \tag{A.8}$$

$$\eta_{nh} = \frac{Ah_n}{M^2}\eta_i^2(M^2 - B')^2 \tag{A.9}$$

where

$$h_p = \frac{D_{pe}}{L_{pe}N_p}\coth\left(\frac{d_p}{L_{pe}}\right) \tag{2.2.5}$$

$$h_n = \frac{D_{nh}}{L_{nh}N_n}\coth\left(\frac{d_n}{L_{nh}}\right) \tag{2.2.6}$$

$$A = \frac{J\tau_{\rm i}}{4qD_{\rm ia}} \tag{2.2.7}$$

By substituting (A.8) and (A.9) into (A.1) and (A.4), and solving with η_i, we obtain,

$$Ah_{\rm p}\eta_{\rm i}^2(M^2+B')^2 - Ah_{\rm n}\eta_{\rm i}^2(M^2-B')^2 + M^2\eta_{\rm i}B' - M^2B = 0 \tag{A.10}$$

$$Ah_{\rm p}\eta_{\rm i}^2(M^2+B')^2 + Ah_{\rm n}\eta_{\rm i}^2(M^2-B')^2 + M^2\eta_{\rm i} - M^2 = 0 \tag{A.11}$$

Eq. (A.10) is added to (A.11). We obtain,

$$2Ah_p(M^2+B')^2\eta_{\rm i}^2 + M^2(1+B')\eta_{\rm i} - M^2(1+B) = 0 \tag{A.12}$$

Eq. (A.10) is subtracted from (A.11). We then obtain,

$$2Ah_n(M^2-B')^2\eta_{\rm i}^2 + M^2(1-B')\eta_{\rm i} - M^2(1-B) = 0 \tag{A.13}$$

By solving (A.12) and (A.13) for η_i and eliminating η_i, we obtain,

$$\frac{h_n(M^2-B')^2}{h_p(M^2+B')^2} = \frac{M(1-B') - \sqrt{M^2(1-B')^2 + 8Ah_n(M^2-B')^2(1-B)}}{M(1+B') - \sqrt{M^2(1+B')^2 + 8Ah_p(M^2+B')^2(1+B)}} \tag{2.2.2}$$

Appendix B. Supplementary material

Supplementary data associated with this article can be found, in the online version, at http://dx.doi.org/10.1016/j.sse.2018.02.014.

References

[1] Hall RN. Power rectifiers and transistors. In: Proceedings of the I.R.E.; 1952. p. 1512–7.

[2] Herlet A. The forward characteristic of silicon power rectifiers at high current densities. Solid-State Electron 1968;11:717–42. http://dx.doi.org/10.1016/0038-1101(68)90053-1.

[3] Baliga BJ. Power semiconductor devices. PWS Publishing Company; 1995. p. 153.

[4] Lutz J. Semiconductor power devices. Springer; 2011. p. 184.

[5] Benda H, Hoffmann A, Spenke E. Switching processes in alloyed pin rectifiers. Solid-State Electron 1965;8:887–906. http://dx.doi.org/10.1016/0038-1101(65)90152-8.

[6] Benda H, Spenke E. Reverse recovery processes in silicon power rectifiers. Proc IEEE 1967;55:1331–54. http://dx.doi.org/10.1109/PROC.1967.5834.

[7] Bellone S, Benedetto LD. An analytical model of the switching behavior of 4H-SiC p+-n-n+ diodes from arbitrary injection conditions. IEEE Trans Power Electron 2012;27:1641–52. http://dx.doi.org/10.1109/TPEL.2011.2164097.

[8] Wei W, Li J, Zhao S. Numerical analysis of reverse recovery characteristics of 4H-SiC p+–n2–n+ power diode with injection conditions. Appl Phys A 2015;118:1387–98. http://dx.doi.org/10.1007/s00339-014-8894-1.

[9] Georgopoulos CJ. Current and voltage waveforms for reverse switching high power p-i-n diodes. IEEE J Solid-State Circ 1976;SC-11:286–95. http://dx.doi.org/10.1109/JSSC.1976.1050716.

[10] Perpiñà X, Jordà X, Vellvehi M, Vobecky J, Mestres N. Analysis of excess carrier concentration control in fast-recovery high power bipolar diodes at low current densities. J Electrochem Soc 2010;157:H711–20. http://dx.doi.org/10.1149/1.3421974.

[11] Yamashita Y, Machida S. Theoretical analysis of forward voltage and reverse recovery charge of silicon p–i–n diodes. Jpn J Appl Phys 2015;54:04DP01. http://dx.doi.org/10.7567/JJAP.54.04DP01.

[12] Rahimo MT. Freewheeling diode reverse-recovery failure modes in IGBT applications. IEEE Trans Indust Appl 2001;37:661–70. http://dx.doi.org/10.1109/28.913734.

[13] Yamashita Y, Machida S. Theoretical analysis of forward voltage and reverse recovery charge of silicon p–i–n diodes. Jpn J Appl Phys 2016;55:04ER01. http://dx.doi.org/10.7567/JJAP.54.04DP01.

[14] Sze SM. Physics of semiconductor devices. 3rd ed. New York: Wiley; 1981. p. 66.

[15] Machida S, Yamashita Y, Sugiyama T. Effects of trap levels on reverse recovery surge of silicon power diode. Jpn J Appl Phys 2013;52:04CP01. http://dx.doi.org/10.7567/JJAP.52.04CP01.

Yusuke Yamashita received B. Eng. and M. Eng. degree in Toyota Technological Institute, Japan, in 2005 and 2007 respectively. He is currently pursuing the Ph.D. degree with the University of Tsukuba, Japan. He also belongs to Toyota Central R&D Labs. Inc. His current research interests focus on power semiconductor devices.

Hiroshi Tadano (M'80) received a Ph.D. degree in semiconductor technology from Tohoku University, Sendai, Japan, in 1980.

In 1980, he joined Toyota Central R&D Labs, Inc., where he was involved in the research and development of power devices such as SIT, IGBT, diodes and power MOSFETs. Since 2013 he has been a professor at the Graduate School of Pure and Applied Science, University of Tsukuba, Tsukuba, Japan. His current research interest is high-efficiency power conversion circuits for electric vehicles using advanced power devices.